Journal of Wind Engineering and Industrial Aerodynamics, 41-44 (1992) 2827–2838
Elsevier

Numerical simulation of boundary layer wind tunnel

T. Maruyama

Disaster Prevention Research Institute Kyoto University, Gokasyo, Uji, Kyoto 611, Japan

Abstract

The boundary layer wind tunnel was simulated numerically. The three-dimensional simulation method of turbulent boundary layer over rough surfaces using a refined k–ε turbulence model was examined and its applicability is shown by comparing the numerical results with experimental data. Using the simulating method described here, wind characteristics over rough surfaces and effect of incident flow on the square cylinder were examined numerically. The good applicability of the simulation results indicate that these preliminary calculations could be a powerful tool in the design of actual wind tunnel tests.

1. INTRODUCTION

A typical experimental arrangement in the boundary layer wind tunnel is shown in Figure 1. Turbulent boundary layers were produced and the incident flows were controlled by using a rough surface placed upwind of object structure models. The flow characteristics vary roughly in three phases from the inlet of test section AD to the outlet BC. These can be divided as flows in the upwind region of the rough surface, the region of the rough surface, and the region downwind of the rough surface. Different calculation methods are required for these regions to compute relevant flow informations. The working section was divided into three computational domains respectively as Domain I, II and III (Figure 1). A grid system[1] and a turbulence model were assigned for each domain appropriately.

Domain I : This is the approach region to the rough surface. The geometry is a rectangular pipe and the numerical solution of this region is basically similar to that of channel flows. The treatment of wall boundary conditions is important. Compared to the other two domains, the flow is rather well suited for computation.

Domain II : This is the region with the rough surface generating a turbulent boundary layer. The flow is markedly affected by the roughness. Therefore, it is crucial to successfully incorporate the effect of the roughness into the calculation. Averagings or approximations could be applied in this region, since usually

0167-6105/92/$05.00 © 1992 Elsevier Science Publishers B.V. All rights reserved.

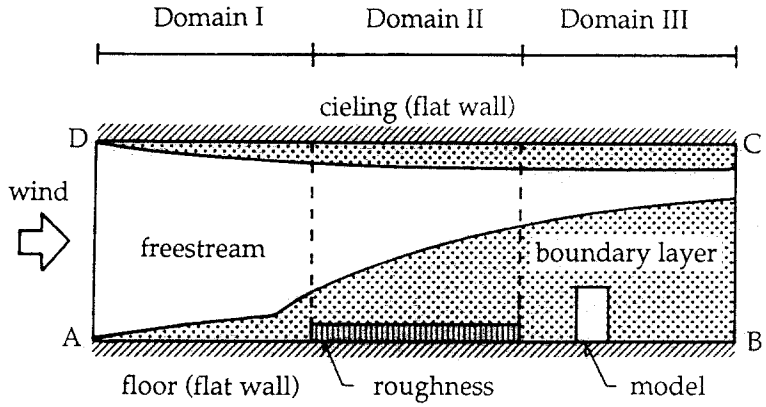

Figure 1. Typical experimental arrangement in the boundary layer wind tunnel.

detailed results such as three-dimensional structure of flows near the roughness elements are not needed. In order to simulate the flow from the floor through the roughness to the top of the boundary layer, a refined k–ε turbulence model[2] was used, and the time-space-averaged values were calculated[3].

Domain III : This is the test section where the objects of the studies such as models of buildings, bridges, mountains, etc. were set up. Detailed simulations are required in this domain. Numerical calculations of the flow around bluff bodies at high Reynolds numbers have been investigated by a number of studies. The simulating method is chosen depending on the aim of study. Time-averaged turbulent flows over three-dimensional rectangular cylinders were computed using a k–ε turbulence model[4]. Unsteady, turbulent flow fields around a cubic model were simulated by means of a large-eddy simulation[5]. To examine detailed structures of eddies around a square cylinder, the unsteady flows were calculated by a direct integration of the incompressible Navier-Stokes equations[6]. The third method is free from error caused by the turbulence modeling.

2. METHOD OF NUMERICAL CALCULATIONS

2.1. Turbulence model

In order to simulate the turbulent boundary layer in the numerical wind tunnel, the performance of the turbulence model is crucial. The model should be able to incorporate the effect of the roughness. To fulfill this requirement the refined k–ε turbulence model[2] was chosen to simulate incompressible turbulent flows with high Reynolds numbers. The set of governing equations under the time-space-averaging on the continuity and the Navier-Stokes equations can be written as follows:

Continuity,

$$\frac{\partial GU_i}{\partial x_i} = 0 \tag{1}$$

Transport of momentum,

$$G\frac{\partial U_i}{\partial t} + \frac{\partial GU_jU_i}{\partial x_j} = -\frac{1}{\rho}\frac{\partial GP}{\partial x_i} - \frac{\partial G\overline{U_iU_j}}{\partial x_j} - GFx_i \tag{2}$$

Transport of turbulent kinetic energy K,

$$G\frac{\partial K}{\partial t} + \frac{\partial GU_jK}{\partial x_j} = \frac{\partial}{\partial x_j}\left(\frac{\nu_t}{\sigma_k}\frac{\partial GK}{\partial x_j}\right) + G\,(S - \varepsilon + F_k) \tag{3}$$

Transport of energy dissipation rate ε,

$$G\frac{\partial \varepsilon}{\partial t} + \frac{\partial GU_j\varepsilon}{\partial x_j} = \frac{\partial}{\partial x_j}\left(\frac{\nu_t}{\sigma_\varepsilon}\frac{\partial G\varepsilon}{\partial x_j}\right) + G\frac{\varepsilon}{K}\,(C_{1E}S - C_{2E}\varepsilon + F_E) \tag{4}$$

Eddy viscosity ν_t

$$\nu_t = \frac{C_\mu K^2}{\varepsilon} \tag{5}$$

and

$$S = -\frac{\overline{U_iU_j}}{G}\frac{\partial GU_i}{\partial x_j} \tag{6}$$

$$\overline{U_iU_j} = -\frac{\nu_t}{G}\left(\frac{\partial GU_i}{\partial x_j} + \frac{\partial GU_j}{\partial x_i}\right) + \frac{2}{3}\,K\delta_{ij} \tag{7}$$

where i,j =1,2,3; x_1 is the streamwise direction x, x_2 is the lateral direction y, x_3 is the vertical direction z; Ui is the x_i-directional component of velocity: U1=U, U2=V, U3=W; ρ, air density; δ_{ij}, the Kroeneker delta, =0 if i≠j and =1 if i=j; P, pressure; t, time. All valuables are time-space-averaged quantities per unit fluid volume, and are nondimensionarized. G is the effective fluid volume defined as the fluid volume against unit volume. G is less than 1.0 within the roughness. The influence of the roughness element is introduced into the transport equations as terms F_{x_i}, F_k and F_E. These were approximated as

$$F_{x_i} = C_{fx_i}a_{x_i}U_i\,|\,U_i\,|\,/2 \tag{8}$$

$$F_k = U_iF_{x_i} \tag{9}$$

$$F_E = K^{3/2}/C_{pE}L \tag{10}$$

where F_{x_i} and C_{fx_i} are the x_i-directional drag caused by roughness and the drag coefficient respectively. The roughness frontal area density a_{x_i} is defined as the ratio of x_i-directional surface area to the fluid volume within the roughness. F_k and F_E are the productions of K and ε due to the roughness. L is the turbulence length scale in the roughness. Since the dominant turbulence scale is assumed to link to the scale of the roughness element, L was set to the quarter of the average value of the length surrounding each roughness element. Hence C_{pE} is the ratio of turbulence scale to L. The values of the model constants from the original model [7] were set equal to those of the standard model and hence,

$$C_D = 0.09,\ \sigma_k = 1.0,\ \sigma_E = 1.3,\ C_{1E} = 1.44,\ C_{2E} = 1.92. \tag{11}$$

This model can incorporate the effect of roughness and simulate the velocity profiles in the layer below the roughness height, which otherwise cannot be expressed such as by conventional logarithmic or power law forms. We can also obtain the streamwise variations of velocity profiles[3]. There are no roughness elements in Domain I and III so that G is 1.0, F_{x_i}, F_k and F_E are set to zero and the turbulence model becomes equivalent to the standard k–ε model.

2.2. Domain decomposition and boundary conditions

The staggered grid system in MAC method[8] was used for discretization. Appropriate configuration of grids were chosen to satisfy the geometry of computational domains and the magnitude of accuracy required. The inlet flow of Domain I was set to uniform flow: U=1.0, V=W=0.0, K=1.0×10^{-5}, ε=6.21×10^{-7}. The calculated values at the downstream of Domain I and II were used as the inlet condition of Domain II and III respectively. The normal gradients of valuables at the downstream boundary were set to zero. At the flat wall boundary such as the floor and the ceiling of the wind tunnel or the walls of test models, the tangential velocity was assumed to obey a power low (the exponent is set to 1/7) and $\varepsilon = C_D^{3/4}K^{3/2}/\kappa\Delta z$ at the first grid points adjacent to the wall, where κ is the Von Karman constant(=0.4) and Δz is the distance of grid points from the wall. The normal velocity and the normal gradient of P, K and ε were considered as zero at the wall. At the surface of the roughness element in Domain II, the flat wall boundary condition was used proportionally to the fraction of the adjacent grid surface that was occupied by the roughness.

2.3. Evaluation of roughness parameters

The drag coefficients C_{fx_i} and the ratio of turbulence scale C_{pE} depend on the configuration of roughness (hereafter C_{fx_i} and C_{pE} are abbreviated as "the roughness parameters"). These values are assumed to be constant in the roughness as long as the roughness configuration does not change. From comparison of the two-dimensional calculations with experimental data, the values of these roughness parameters were optimized to fit the calculated results

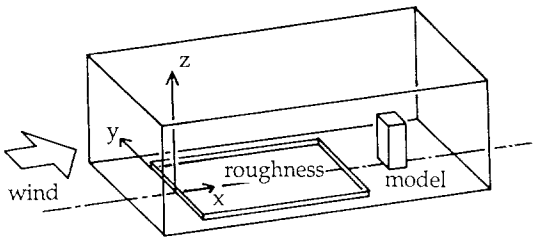

Figure 2. Experimental arrangement and coordinate system.

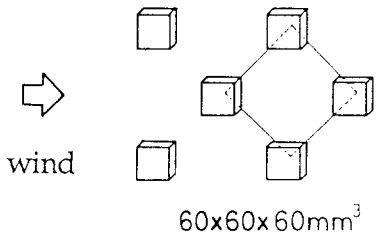

Figure 3. Configuration of roughness.

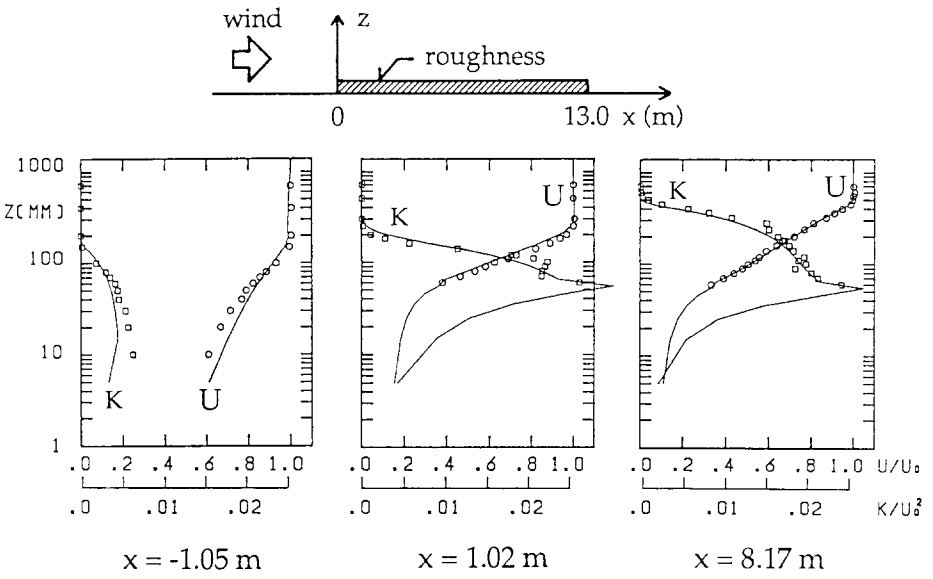

Figure 4. Comparison of two-dimensional calculation values with experimental data at various positions: experimental data,○,U; □,K; calculated values — ; U_0 is the freestream velocity; G=0.875, C_{fx}=1.90, a_x=2.38(1/m), C_{fz}=0.0, a_z=0.0(1/m), C_{pE} =0.40.

with the experiments for various roughness configurations. The governing equations were approximated by a finite difference scheme to simulate the two-dimensional flow. The Adams-Bashforth scheme was employed for time-marching. Numerical integrations were conducted according to the SMAC method[9]. The experimental arrangement and the coordinate system are shown in Figure 2. Examples of comparison for the roughness presented in Figure 3 are shown in Figure 4.

3. SIMULATION OF TURBULENT BOUNDARY LAYER

Three-dimensional simulations were carried out using the values of the roughness parameters obtained from the two-dimensional calculations. The calculation method was slightly different from that used in the two-dimensional simulation in order to reduce the load of computation. The Euler scheme was employed for time-marching and the ABMAC method[10] was used for numerical integrations. Simulated results of Domain II with the rough surface presented in Figure 3 and Domain III without structure models are shown Figure 5, 6 and 7. The development of turbulent boundary layer is shown in these figures. At the upwind edge of the rough surface, the upward velocity increased, and a large amount of turbulent kinetic energy was generated. The turbulent energy convected according to the development of the turbulent boundary layer. At the downwind edge, downward velocity increased and the streamwise velocity near the floor increased as it goes further downstream. Calculated values of U and K were compared with experimental data in Figure 8. The simulated values match fairly well with the experimental data.

4. NUMERICAL WIND TUNNEL TEST

Many kinds of turbulent boundary layers can be created in the numerical wind tunnel using various roughness parameters and arrangements of the rough surface in the computational domains. Numerical experiments were tested on a square cylinder using various incident flows and by varying the height of cylinder. The cylinder 10 cm by 10 cm in cross-section was located on the center line in Domain III as shown in Figure 9.

4.1. Effect of the incident flow profile

The effect of the profile was examined using different incident flows. Three flows A, B and C that have the same thickness were generated numerically as shown in Figure 10. The vertical gradient of velocity and the turbulent kinetic energy increases in the order of A, B and C. The cylinder 30 cm high was tested.

Variations of the pressure distributions on the frontal wall are shown in Figure 11. The pressure was presented by the pressure coefficient $C_p=(p-p_o)/(\rho U_o^2/2)$, where p is the pressure on the wall, p_o is the reference pressure and U_o the incident velocity at a height of cylinder as shown in Figure 9. The patterns of pressure distribution varied with the incident flows as shown in Figure 11. The high pressure region moved upward and the maximum value of pressure increased with the increase of the wind gradient of incident flow.

4.2. Effect of incident flow thickness

Three flows D, E and F with different thickness as shown in Figure 12 were generated using the same roughness parameters. A cylinder 50 cm high was tested. Variations of the pressure distributions on the frontal wall are shown in Figure 13. The high pressure region moved upward as the thickness increased. A

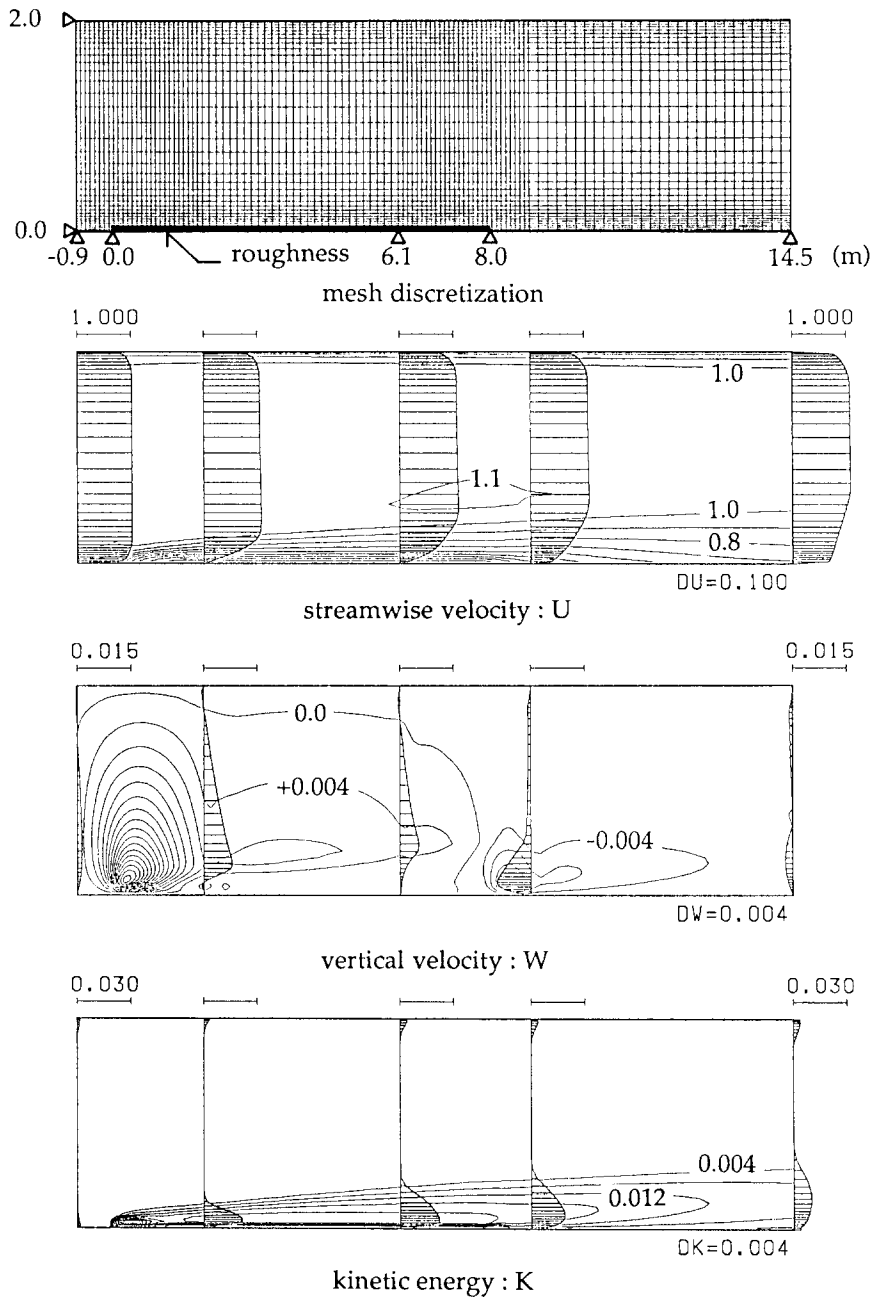

Figure 5. Distributions and profiles of simulated values in x-z planes at y=0.0 m.

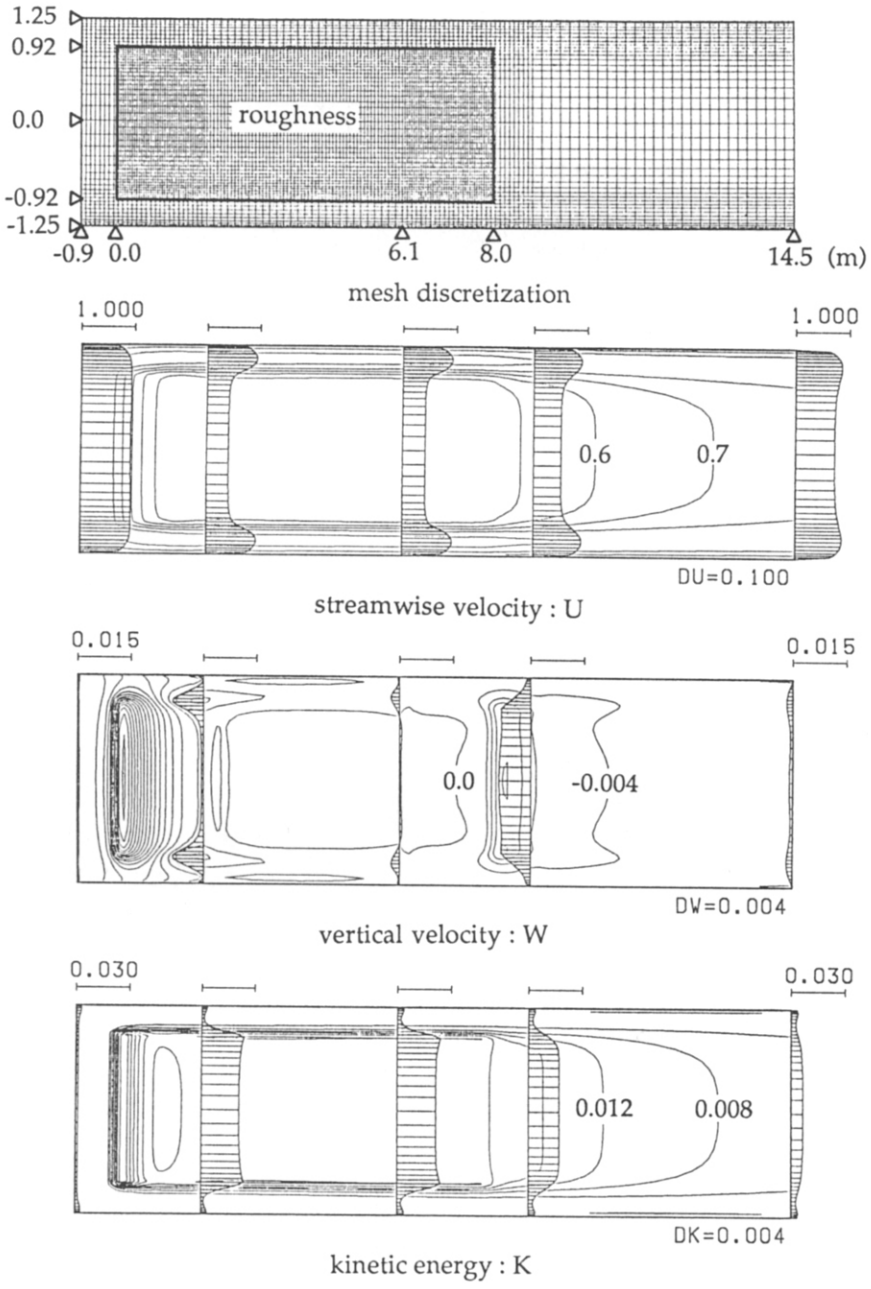

Figure 6. Distributions and profiles of simulated values in x-y planes at z=.035 m.

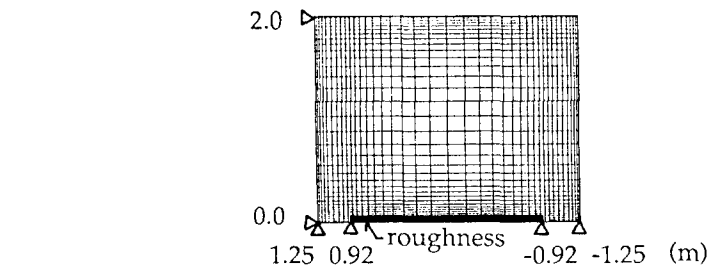

mesh discretization

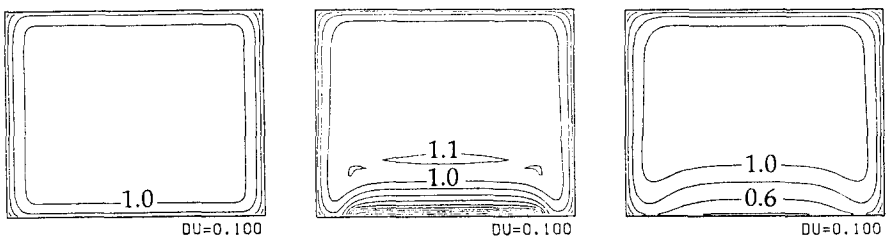

x = -0.9 m x = 6.1 m x = 14.5 m

streamwise velocity : U

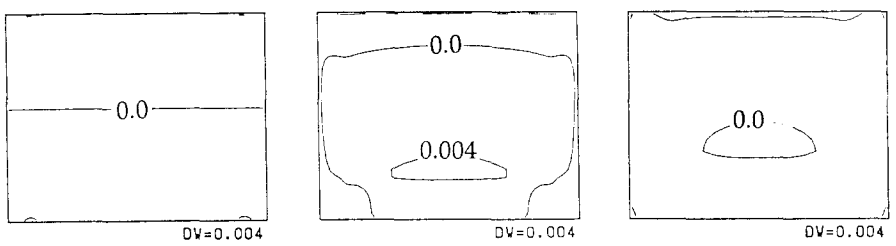

x = -0.9 m x = 6.1 m x = 14.5 m

vertical velocity : W

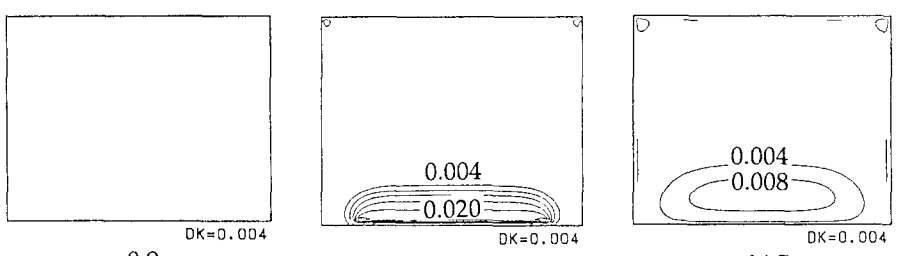

x = -0.9 m x = 6.1 m x = 14.5 m

kinetic energy : K

Figure 7. Distributions of simulated values in y-z planes at various positions.

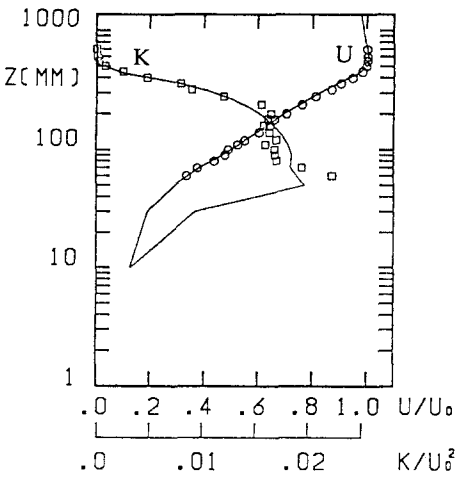

Figure 8. Comparison of three-dimensional calculation values with experimental data at x=7.44(m), y=0.0(m): experimental data,○,U; □,K; calculated values — . U_o is the freestream velocity; G=0.875, C_{fx}=1.90, a_x=2.38(1/m), C_{fz}=0.0, a_z=0.0(1/m), C_{pE}=0.40.

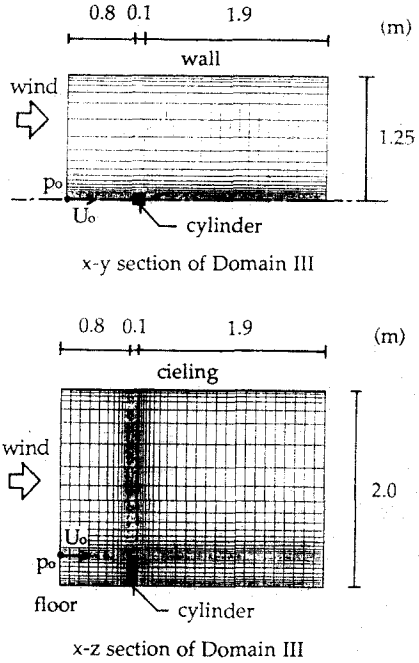

Figure 9. Location of cylinder and mesh discretization.

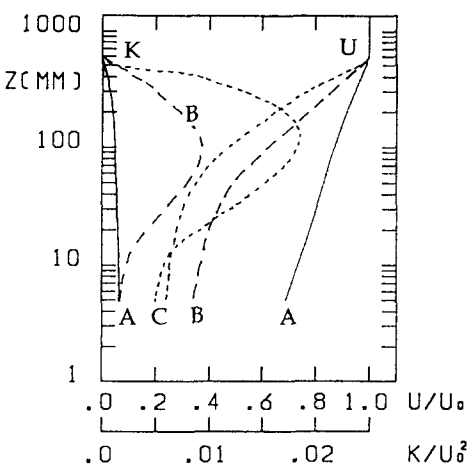

Figure 10. Variation of incident flow profiles at y=0.0 m.

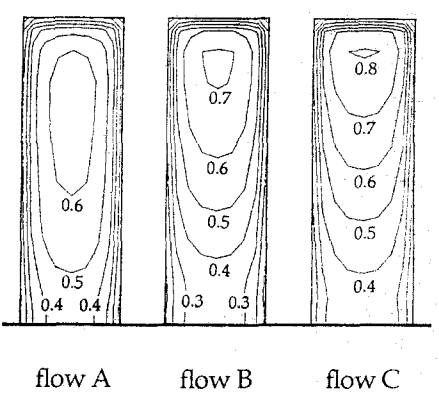

Figure 11. Variation of pressure distributions on the frontal wall with the incident flow profiles.

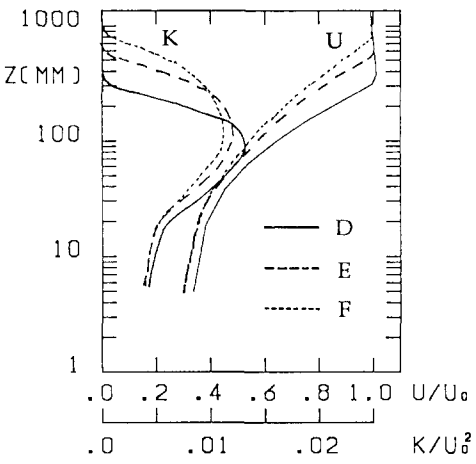

Figure 12. Variation of thickness of incident flows at y=0.0 m.

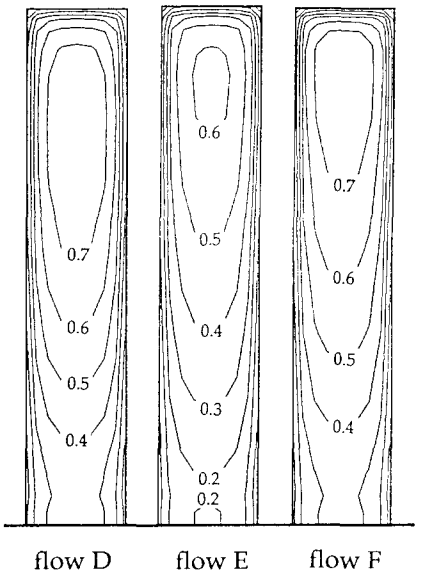

Figure 13. Variation of pressure distributions on the frontal wall with the thickness of incident flows.

drop of the maximum value of the pressure was observed in the flow E.

Here the comparisons of pressure distributions on the walls of the cylinder were performed only on the frontal wall because the k–ε turbulence model used in this study cannot simulate the wake region properly[11]. The Reynolds-stress turbulence model, large-eddy simulation or direct simulation will be recommendable for detailed analyses on the flows around the cylinder. On the other hand, rough estimates derived from the k–ε turbulence model is useful for the design of actual wind tunnel tests, and the method of generating turbulent boundary layers presented here is also practical to create the incident flow conditions.

5. CONCLUSION

The boundary layer wind tunnel was simulated numerically. The three-dimensional simulation method of turbulent boundary layer over a rough surface using a refined k–ε turbulence model was examined and its applicability was shown by comparing the numerical results with experimental data.

Using the simulating method described here, the following problems were examined numerically:

(a) Wind characteristics of turbulent boundary layers over rough surfaces,
(b) Effect of characteristics of incident flow (profiles, thickness of boundary layer) on the square cylinder,

These were shown to be expressed relevantly. Such prior preliminary calculations obtained in numerical wind tunnels will be of great help for the design of actual wind tunnel tests.

There are still many problems in reproducing the same performance as the actual wind tunnels by simulations. If advanced simulations using more strict calculation methods or reliable turbulence models can be developed, it is possible that these simulations can replace wind tunnel tests at least in some areas.

Acknowledgments

The author is grateful to Mr. H.Hiraoka (assistant of Kyoto University) for his advice and kind guidance for the development of programs.

REFERENCES

1 T. Kajimoto and N. Satofuka, Trans. J.S.M.E., B55-518 (1989) 3006 (in Japanese).
2 H. Hiraoka, T. Maruyama, Y. Nakamura and J. Katsura, Planning and Environmental Eng. (Trans. A.I.J.), 400 (1989) 1 (in Japanese).
3 T. Maruyama, J. Structural and Construction Eng. (Trans. A.I.J.), 404 (1989) 75 (in Japanese).
4 D.A. Paterson and C.J. Apelt, J. Wind Eng. Ind. Aerodyn., 24 (1986) 193.
5 S. Murakami and A. Mochida, J. Wind Eng. Ind. Aerodyn., 25 (1987) 291.
6 T. Tamura and K. Kuwahara, J. Wind Eng. Ind. Aerodyn., 33 (1990) 161.
7 B.E. Launder and D.B. Spalding, Lecture in Mathematical Models of Turbulence, Academic Press (1972).
8 F.H. Harlow and J.E. Welch, The Physics of Fluid, 8 (1965) 2182.
9 A. Amsden and F.H. Harlow, The SMAC method, Los Alamos Scientific Laboratory, (1970).
10 J.A. Viecelli, J. Computational Physics, 8 (1971) 119.
11 S. Murakami, A. Mochida and Y. Hayashi, J. Wind Eng. Ind. Aerodyn., 35 (1990) 87.